

Computed Tomography Protocol Optimisation for Pediatric Head Trauma: Radiation Dose and Image Quality Assessment

Evelyn Anaafi^{1,2}, Mary Boadu¹, Albertina Rusandu³,
Mercy Afadzi⁴, Kwame Anokye Amoabeng^{1,5*}

¹Department of Medical Physics, Graduate School of Nuclear and Allied Sciences, University of Ghana, Legon

²Sweden-Ghana Medical Center, Accra, Ghana

³Department of Circulation and Medical Imaging, Norwegian University of Science and Technology (NTNU), Trondheim, Norway

⁴Department of Physics, Norwegian University of Science and Technology (NTNU), Trondheim, Norway

⁵National Centre for Radiotherapy and Nuclear Medicine, Korlebu Teaching Hospital, Accra, Ghana

Email: *amoabengkwameanokye@gmail.com

How to cite this paper: Anaafi, E., Boadu, M., Rusandu, A., Afadzi, M. and Amoabeng, K.A. (2022) Computed Tomography Protocol Optimisation for Pediatric Head Trauma: Radiation Dose and Image Quality Assessment. *International Journal of Medical Physics, Clinical Engineering and Radiation Oncology*, 11, 160-175.

<https://doi.org/10.4236/ijmpcero.2022.113014>

Received: July 9, 2022

Accepted: August 20, 2022

Published: August 23, 2022

Copyright © 2022 by author(s) and

Scientific Research Publishing Inc.

This work is licensed under the Creative

Commons Attribution International

License (CC BY 4.0).

<http://creativecommons.org/licenses/by/4.0/>



Open Access

Abstract

Purpose: Children are sometimes examined with Computed Tomography protocols designed for adults, leading to radiation doses higher than necessary. Lack of optimisation could lead to image quality higher than what is needed for diagnostic purposes with associated high doses to patients. Optimising the protocols for paediatric head trauma CT imaging will reduce radiation dose. **Objective:** The study aimed to optimise radiation dose and assess the image quality for a set of protocols by evaluating noise, a contrast to noise ratio, modulation transfer function and noise power spectrum. **Methods:** Somatom Sensation 64 was used to scan the head of an anthropomorphic phantom with a set of protocols. ImageJ software was used to analyse the paediatric head image from the scanner. IMPACTSCAN dosimeter software was used to evaluate the radiation dose to the various organs in the head. MATLAB was used to analyse the Modulation Transfer Function and the Noise Power. **Results:** The estimated Computed Tomography Dose Index volume (CTDI_{vol}) increased with increasing tube current and tube voltage. The high pitch of 0.9 gave a lower dose than the 0.5 pitch. The eye lens received the highest radiation dose (39.2 mGy) while the thyroid received the least radiation dose (13.7 mGy). There was an increase in noise (62.46) when the H60 kernel was used and a lower noise (8.829) was noticed when the H30 kernel was used. **Conclusion:** The results obtained show that the H30 kernel (smooth kernel) gave higher values for noise and contrast to noise ratio (CNR) than the H60 kernel (sharp kernel). The H60 kernel produced high

values for the modulation transfer function (MTF) and noise power spectrum (NPS). The eye lens received the highest radiation dose.

Keywords

Image Quality, Radiation Dose, Modulation Transfer Function, Noise Power Spectrum, Optimization

1. Introduction

The utilization of Computed Tomography (CT) in paediatric imaging has expanded throughout the most recent years, and it has been quickly expanding since its presentation in the 1970s [1]. The advancement of this modality from single-detector to multi-detector and the possibility for helical scanning has provided many advantages in clinical settings, which has made CT the preferred option for several clinical indications [2]. Cranial computed tomography is a reliable imaging method for identifying intracranial lesions in patients with head trauma [3].

According to Hagel [4], tube current reduction based on age, size and weight was formerly used to optimize radiation dose in children. But currently, the use of lower radiation energy is of more interest since it has shown that higher tube voltage increases radiation doses in paediatrics without necessarily improving image quality [5]. The practice of as low as reasonably achievable (ALARA) principle thus optimization and justification can result in minimization of unnecessary exposure from CT examinations in paediatric head trauma imaging.

CT image quality is a composite of many different factors of both observed and physical quantities like modulation transfer function (MTF), a contrast to noise ratio (CNR), uniformity, CT numbers and noise [6]. It is the differential absorption and attenuation of X-ray beams that provide the contrast used in radiographs and CT to distinguish between grey and white matter, haemorrhage and brain [7]. To obtain an image with a higher quality, it is significant to interpret and obtain the highest information from the images. Determination of optimal image quality is a complex task involving both quantitative objective physical measures linked with subjective observer perceptions as an indication of clinical performance [8]. CNR is the ability to visualise different tissues through the noise. MTF determines how much contrast in an original object is maintained by the detector. CT number is the Hounsfield unit. Noise describes any content of an image that limits the ability to visualize lesions or pathology. CT image quality is sometimes affected by the image reconstruction algorithms used [9].

In paediatrics, the head is the most imaged body part. There have been concerns about radiation doses from CT since the early 2000s, focusing on paediatric CT with subsequent articles raising concern for potential carcinogenesis from medical imaging [10]. A study that directly assessed the risk of cancer after CT scans in children found a clear dose-response relationship for both leukaemia

and brain tumour: the risk increased with increasing cumulative radiation dose [11]. Minimization of radiation dose associated with paediatric CT examination is of particular importance because the risk due to radiation exposure is two to three times greater than the risk for adults [12].

Therefore, the CT protocols used to image adults should be different from that of children because the cells of children are rapidly dividing and are more sensitive and vulnerable to the effects of ionizing radiation. According to Naumann [13], comprehensive CT dose standards exist for adults, but are incomplete for children. It has been a complicated challenge controlling exposure to medical imaging. Paediatric head trauma protocols should be different from other head indications protocols to avoid unnecessary radiation. Much attention should be focused on CT paediatric protocol review and optimization, to reduce radiation dose.

The study aimed to optimise paediatric CT head trauma protocols and assess image quality by measuring noise, contrast resolution, spatial resolution and noise power spectrum and study their effect on radiation dose.

2. Materials and Methods

2.1. Computed Tomography Scanner

Siemens Somatom Sensation 64 CT scanner was used (see **Figure 1**). This machine



Figure 1. The Siemens Somatom Sensation 64 CT scanner.

offers a high routine isotropic resolution of 0.33 mm, allowing it to visualise the smallest pathology and offers an exceptional 0.24 mm isotropic resolution. It has an image reconstruction matrix of 512 * 512 and reconstruction time of 0.06 s per image. It has a maximum scan time of 100 s depending on the pitch, mAs and kVp with a spatial resolution of 30 Ip/cm.

2.2. Catphan 600

The Catphan 600 phantom (Phantom Laboratory Incorporated, USA) was used for the objective image quality assessment by measuring the noise, spatial resolution, CT-numbers and contrast resolution.

2.3. The Anthropomorphic Phantom

A 5-year-old anthropomorphic phantom was used in this study (manufactured by the Kyoto Kagaku). According to Ramos [14], anthropomorphic phantoms are built from tissue equivalent materials that represent the anatomy of the human body and give attenuation characteristics. The head of the whole-body phantom PBU-70 was used.

The Catphan 600 phantom was positioned on the couch and aligned with the lasers. Twenty-seven (27) test images and one reference image were obtained using different exposure techniques. H30 kernel was used to smoothen the images and reduce visible image noise and improve contrast resolution. H30 displays body part with inherently small contrast resolution; this gives a better assessment of the brain. High spatial frequency algorithm, H60 kernel was used to increase the image sharpness at the expense of increased noise. This algorithm is used to display bony parts with inherently wide object contrast. The filtered back projection was used as the post-processing algorithm. The field of view used was 210 cm and was maintained throughout the work. A slice thickness of 4 mm was used for all the exposures with a rotation time of 1s. The reference parameter used was 120 kVp and 250 mAs. The head of the anthropomorphic phantom was scanned with the same acquisition protocols used for the catphan.

2.4. Exposure Parameters

The exposure parameters used to acquire images from the catphan and anthropomorphic phantoms were kVps of 120, 100 and 80; mAs of 300, 250, 230, 210, 190; pitch of 0.5 and 0.9. These exposure parameters were selected based on the commonly used diagnostic exposure factors in ten major hospitals in Ghana. For each kVp, images were acquired by varying the mAs and the pitch as shown in **Table 1**.

2.5. Image Quality Assessment/Evaluation

Image quality indicators that were assessed include CT numbers, homogeneity, uniformity, contrast to noise ratio, noise power spectrum and the modulation transfer function.

2.5.1. Noise

The noise was calculated by setting a region of interest (ROI) of size 40% of the original size on the selected images from the picture archiving communication system (PACS) (see **Figure 2**).

$$\text{Noise} \propto \frac{1}{\sqrt{mAs}} \quad (1)$$

Table 1. Exposure parameters used for the acquisition of anthropomorphic and Catphan phantom images.

kVp	mAs	Pitch
120	250	0.5
120	250	0.9
120	230	0.5
120	230	0.9
120	210	0.5
120	210	0.9
120	190	0.5
120	190	0.9
100	300	0.5
100	300	0.9
100	250	0.5
100	250	0.9
80	300	0.5
80	300	0.9

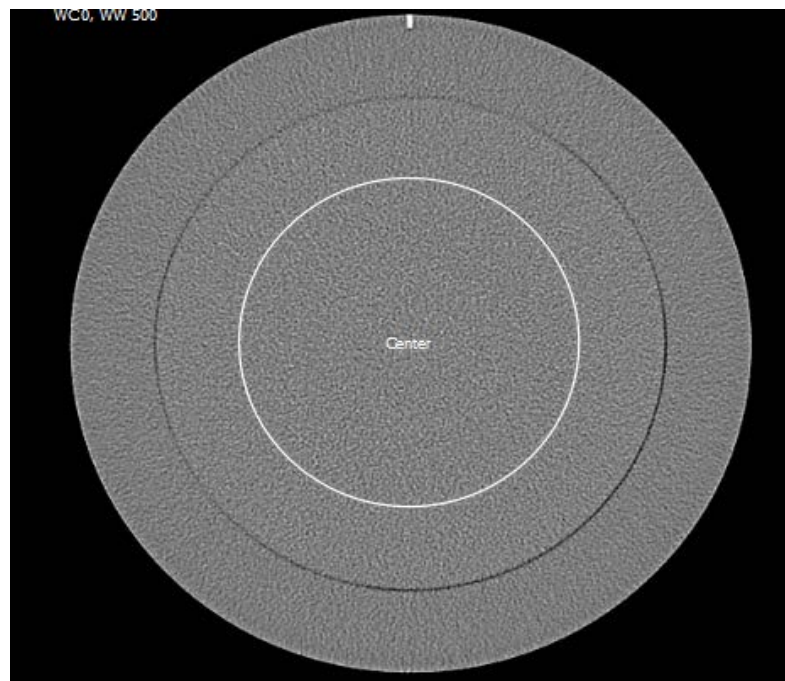


Figure 2. Representative image for evaluating noise obtained with the catphan phantom.

2.5.2. Contrast to Noise Ratio (CNR)

A region of interest (ROI) was drawn in the largest target inside the low contrast module as shown in **Figure 3**. The same size of ROI was drawn close to this target to serve as the background.

$$\text{CNR} = \frac{2(HU_m - HU_b)^2}{SD_m^2 + SD_b^2} \quad (2)$$

where HU_m is the mean HU of the area of interest in the material and HU_b is the mean HU of the background area and SD_m is the standard deviation of the area of interest in the material and SD_b is the standard deviation of the background. A higher CNR, corresponds to better image quality.

2.5.3. CT-Numbers

The Catphan 600 has inserts made of Teflon, acrylic, low-density polyethylene (LDPE), polymethylpentene (PMP), derlin, polystyrene and air. The CT numbers were measured manually by placing the ROI within the inserts in the CT images (see **Figure 4**).

2.5.4. Noise Power Spectrum

Noise power spectrum is not only affected by the amount of noise present, but also by the noise structure, thus the amount of noise appears as the area under the Noise Power Spectrum (NPS) curve, while the shape of the curve shows characterises the noise structure (see **Figure 5**).

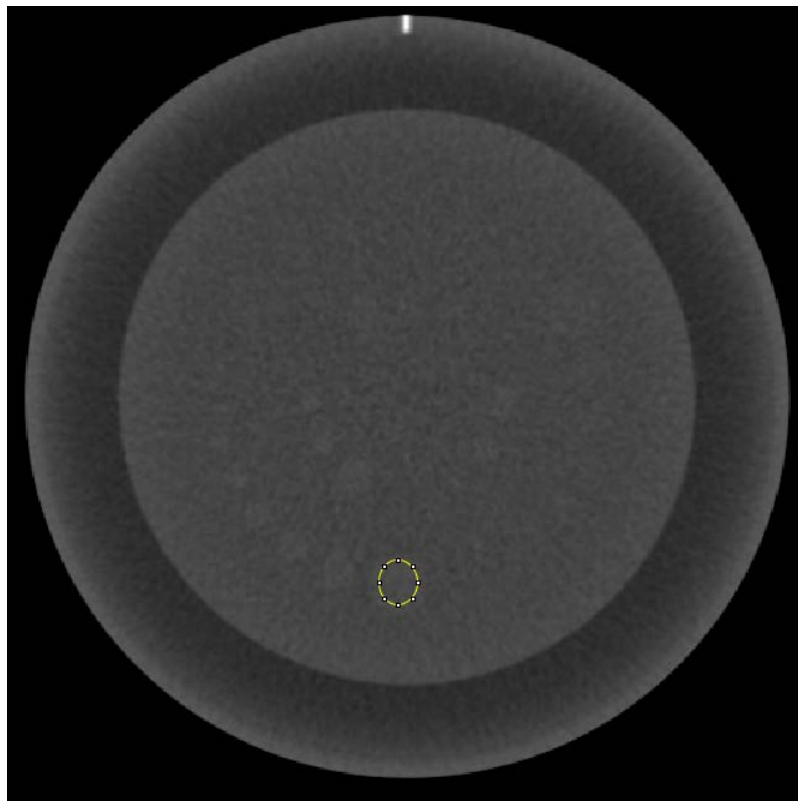


Figure 3. A representative image of CNR.

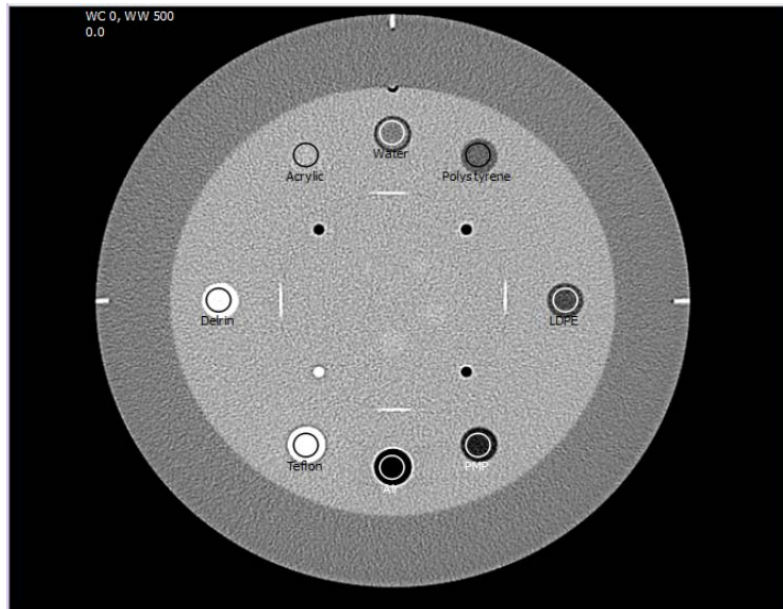


Figure 4. An image of the sensitometry insert.

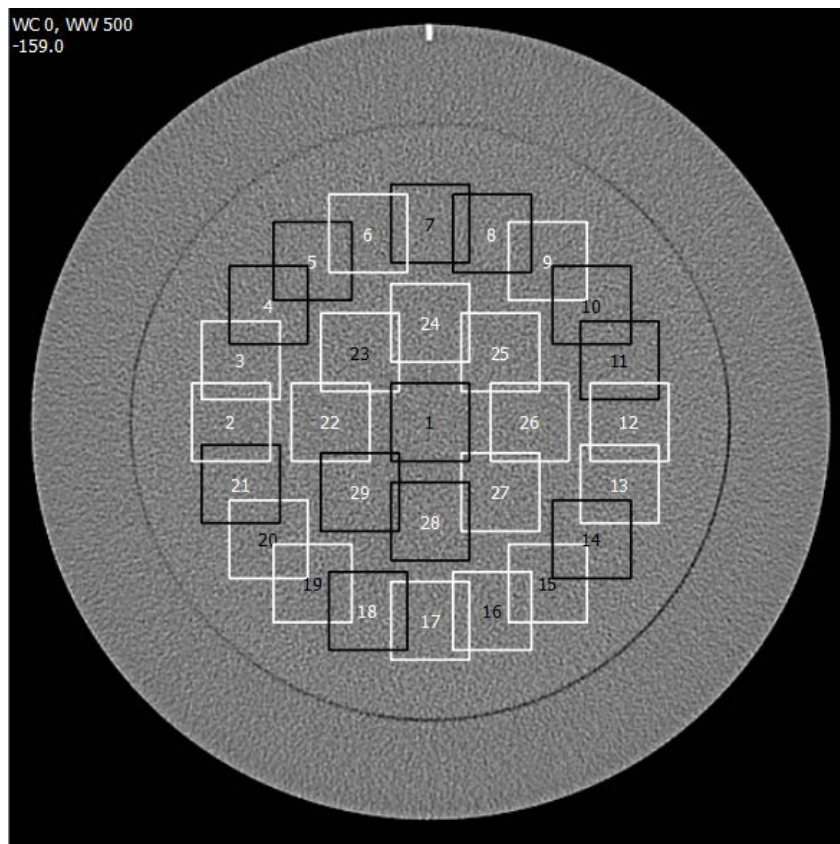


Figure 5. An image of uniformity in the catphan.

3. Results

The results include $CTDI_{vol}$, noise, low contrast resolution, noise power spectrum, modulation transfer function and CT number.

3.1. Results of mAs and CTDI_{vol} Using a Pitch of 0.5 and 0.9

Figure 6 shows an increase in CTDI_{vol} values with increasing mAs for pitches of 0.5 and 0.9. Also, the 0.9 pitch measured lower dose values by a percentage reduction of 2.3% than the 0.5 pitch.

3.2. Radiation dose and Image Quality

3.2.1. Noise

It was observed that the H30 kernel gives a lower noise compared with the H60 kernel (see **Figure 7(a)** and **Figure 7(b)**). However, there was no significant difference in noise when the pitch was changed from 0.5 to 0.9. There was an average of 2.3% reduction in CTDI_{vol} when the pitch was changed from 0.5 to 0.9. There was a strike balance between noise (5.49) and CTDI_{vol} at 28.3 mGy.

3.2.2. Contrast to Noise Ratio

In **Figure 8(a)**, a steady increase in CNR was observed with increasing CTDI_{vol} but decreased after 29.8 mGy at the CNR increased. Also, the H60 kernel measured lower values of CNR than the H30 kernel which measured a significantly higher CNR values. The H60 kernel showed a linear increase in CTDI_{vol} with no significant change in the CNR. The H30 kernel increased non-linearly in the CNR values as the CTDI_{vol} increased. At a CNR of 5.282 and a CTDI_{vol} of 39.1 mGy, there was a strike balance between image quality and radiation dose. From **Figure 8(a)** and **Figure 8(b)**, there was a 26.6% reduction in dose when the protocol was reduced from 120 kVp 250 mAs to 120 kVp 190 mAs.

3.2.3. Modulation Transfer Function

From **Figure 9(a)**, at 50% spatial frequency, MTF was constant as the CTDI_{vol} increased. While at 10%, the MTF sharply increased to 1.08 at 23.7 mGy CTDI_{vol}. However, there were no significant variations in MTF (1.02 to 0.98) when the

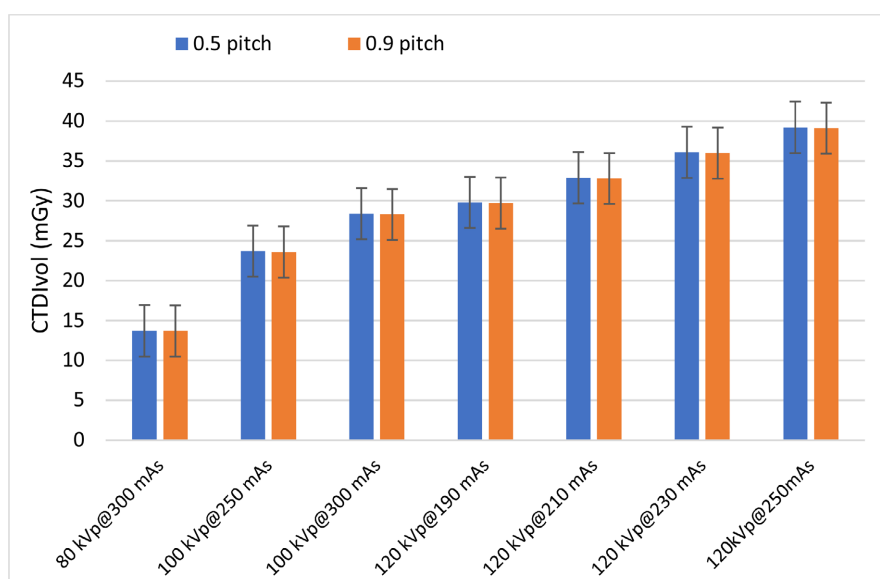


Figure 6. A graph of CTDI_{vol} against mAs.

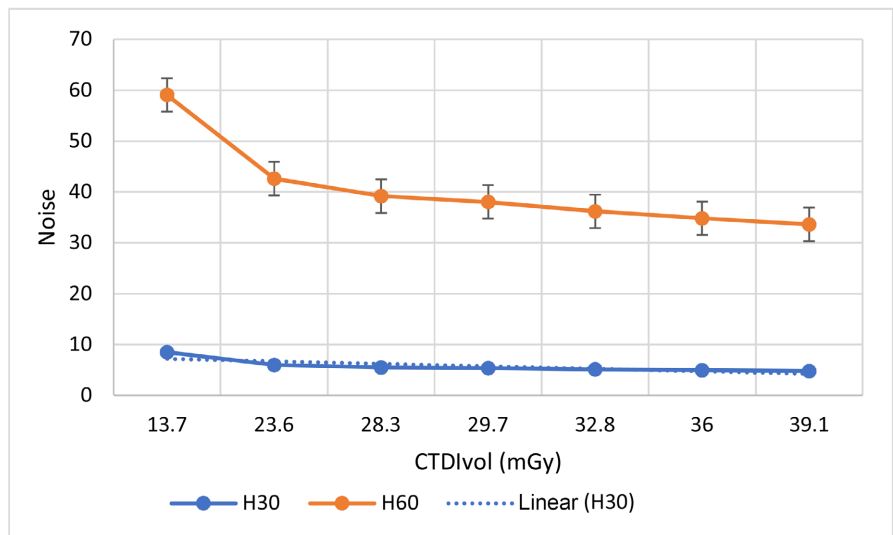
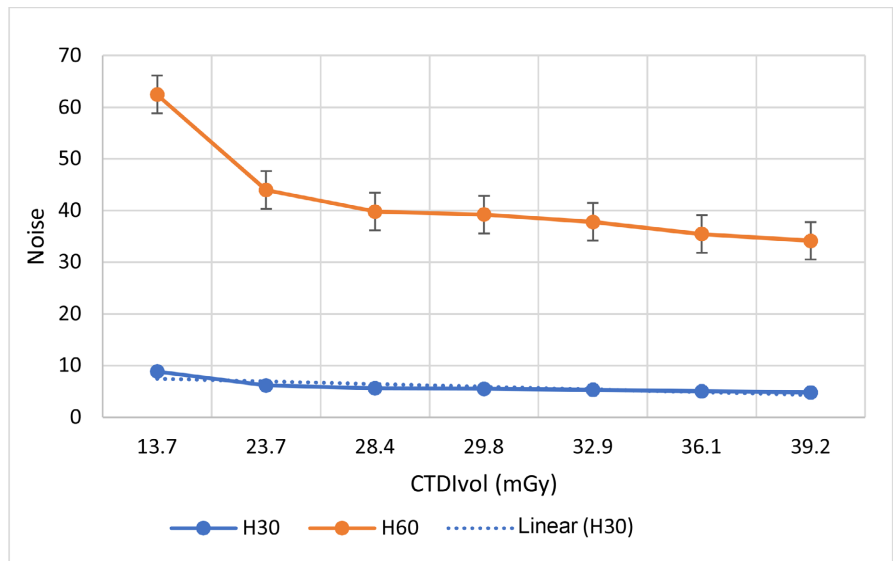
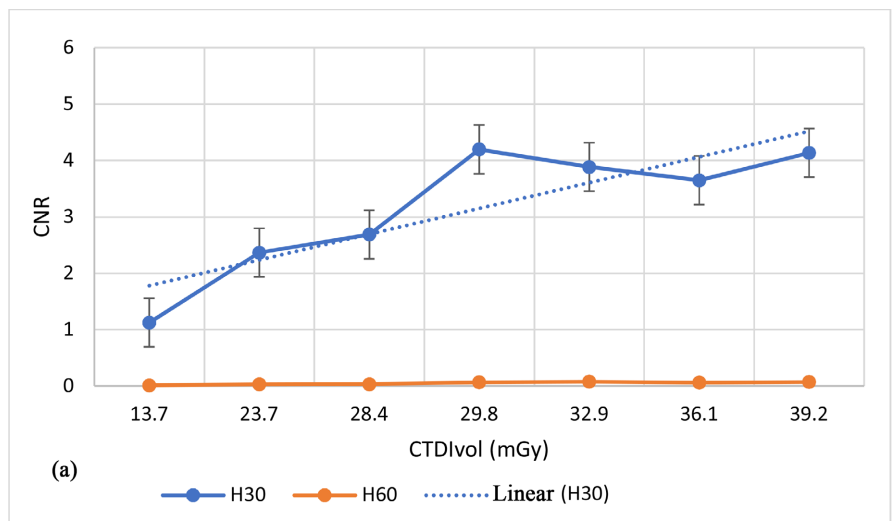


Figure 7. Graph of noise and CTDI_{vol} using H30 and H60 kernel with (a) a pitch of 0.5 and (b) a pitch of 0.9.



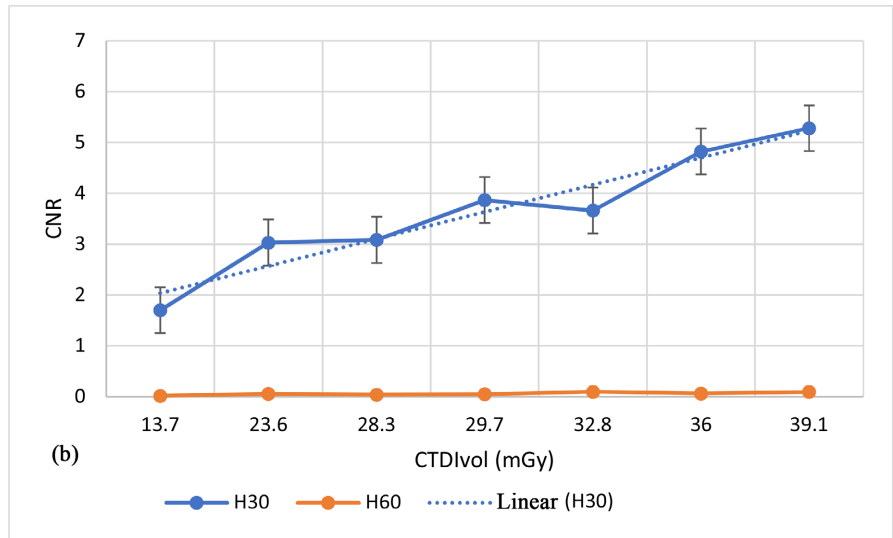


Figure 8. A graph of CNR and CTDI_{vol} (mGy) using H30 and H60 kernels (a) with a pitch of 0.5 and (b) with a pitch of 0.9.

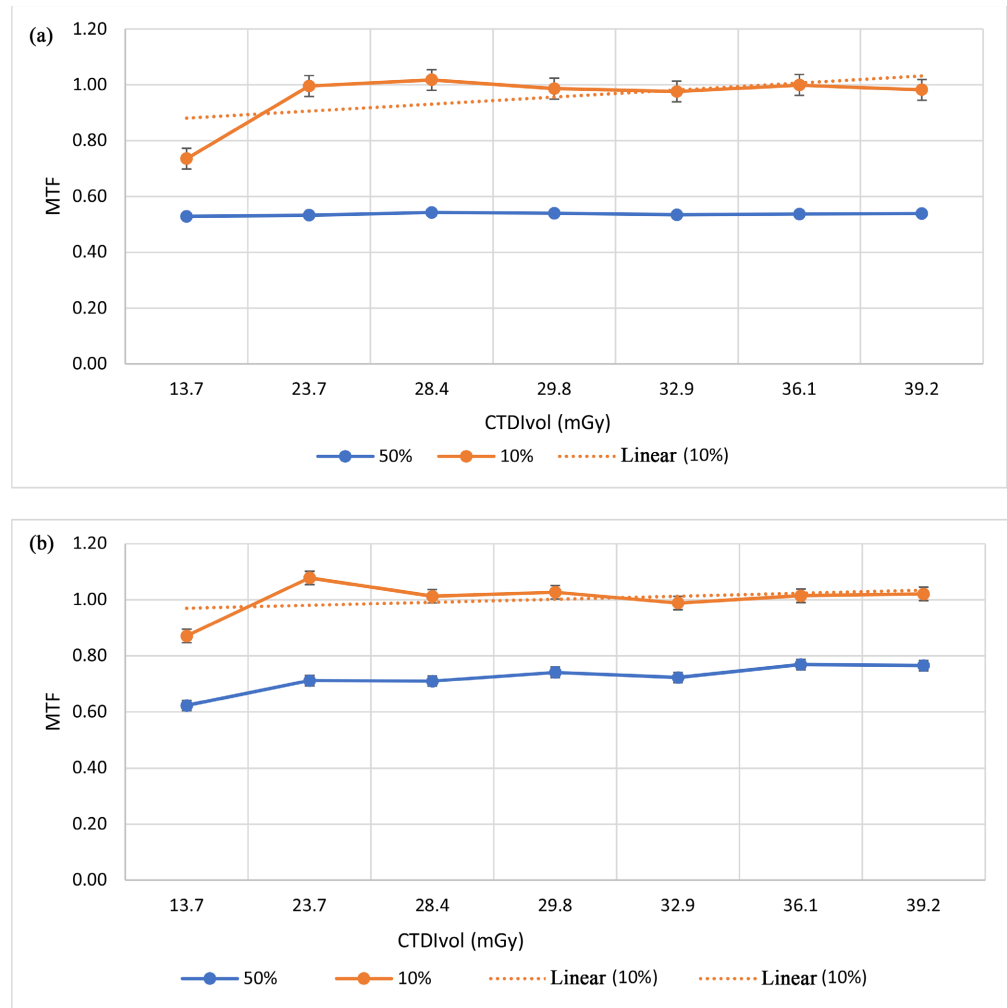


Figure 9. A graph of MTF and CTDI_{vol} with a pitch of 0.5 using (a) H30 kernel and (b) H60 kernel and a spatial frequency of 50% and 10%.

dose was increased from (28.4 to 39.2) mGy. In **Figure 9(b)**, there was no variation in MTF at 50% spatial frequency with dose. While at 10% there was an increase in MTF as the $CTDI_{vol}$ increased.

3.2.4. Noise Power Spectrum

It was observed that the H60 kernel was skewed to the right while the H30 kernel was skewed to the left (see **Figure 10**).

3.3. Results of Organ doses Using Different Pitch

Figure 11(a) and **Figure 11(b)** give the results of organ doses using a pitch of 0.5 and 0.9 respectively.

A tube voltage of 120 kVp and tube current of 190, 210, 230 and 250 mAs were used for the two different pitches.

As shown in **Figure 11(a)** and **Figure 11(b)**, organ dose increased with increasing $CTDI_{vol}$ in both 0.5 and 0.9 pitches. There was 45.0% reduction in organ doses when the pitch was changed from 0.5 to 0.9.

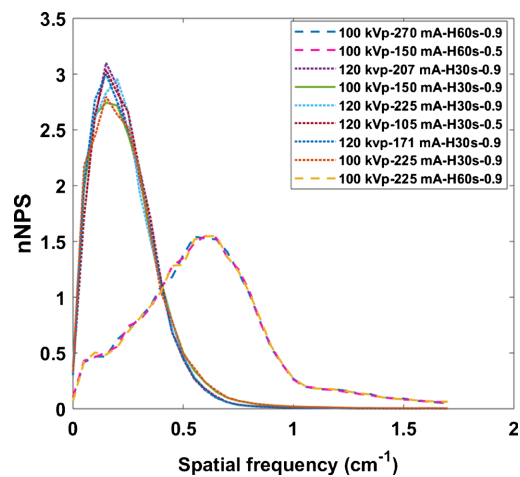
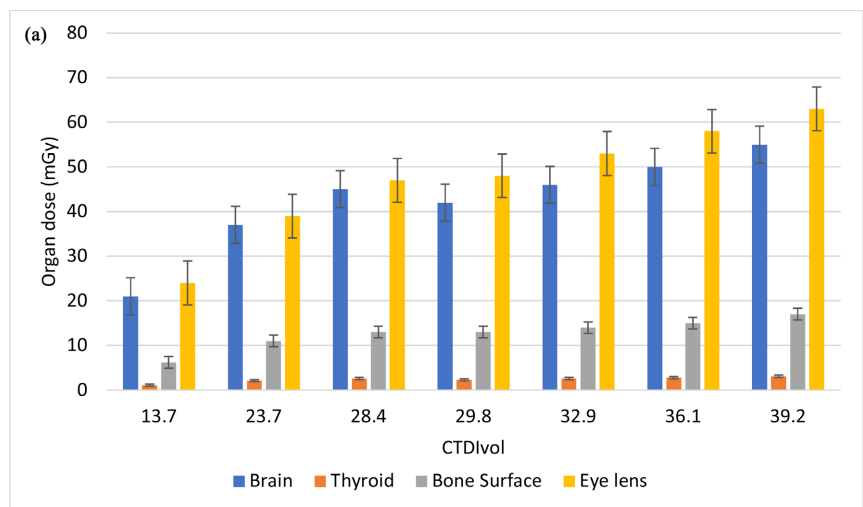


Figure 10. A graph of nNPS and spatial frequency with a pitch of 0.5 and 0.9 using H30 and H60 kernels.



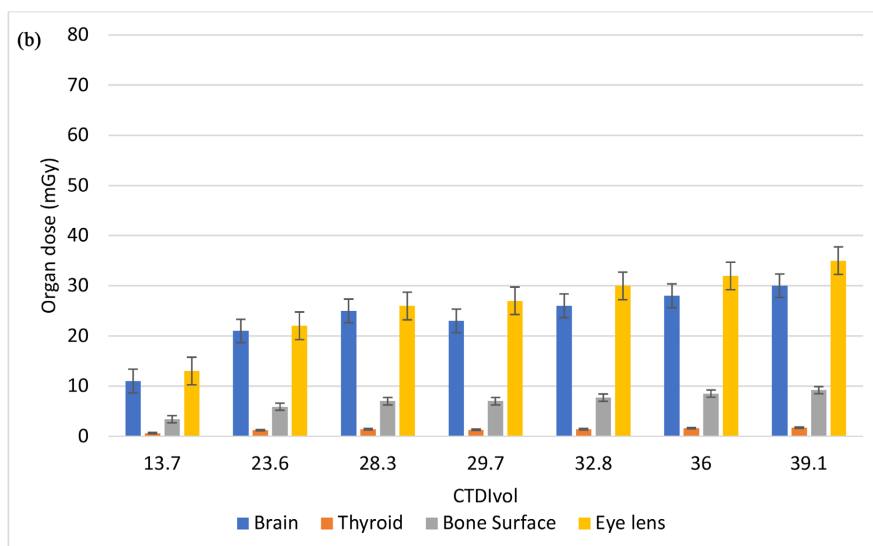


Figure 11. A graph of organ dose and CTDI_{vol} using the pitches 0.5 and 0.9.

4. Discussion

As mAs increased, CTDI_{vol} also increased and this is consistent with a study by Gundogdu *et al.* [15], where a 50% reduction in mAs produced a 40% increase in noise, degrading image contrast and reducing dose by 50%. This is consistent with Hanan *et al.* [16], who found that an increase in mAs and kVp increases image noise. A 17% reduction in the mAs decreased the CTDI_{vol} by 17%. This agrees with Zhang *et al.* [17], who observed that a decrease (20% - 33%) in mAs produced the same percentage decrease in CTDI and dose length product (DLP) (20% - 33%) and confirmed the linear relationship between mAs and dose.

There was an increase of 83.6% in noise when the kernel was changed from H30 to H60. This shows that the sharp kernel (H60) is not good for imaging organs with low contrast organs like the brain since it produces images with more noise. From **Figure 7(a)**, there was an increase in noise as dose decreased in both the H30 and H60 kernels which reduced image quality. This agrees with Choi [18], who stated that a decrease in dose in a paediatric abdominal CT scan would cause a high level of noise and reduce image quality. There was almost no change in noise (5.593) at 28.4 and 29.8 mGy as CTDI_{vol} increased. Increasing the CTDI_{vol} reduces image noise as illustrated in **Figure 7(a)** and **Figure 7(b)**.

CNR is greatly degraded by noise. Hence, a decrease in CTDI_{vol} will lead to a decrease in CNR due to increased noise at lower doses. A lower kVp enhances CNR, nevertheless, the lowest CNR was recorded at the lowest kVp. A 98% decrease in CNR was observed when the kernel was changed from H30 to H60. This agrees with Yu [19], who estimated that the CNR is largely affected by the reconstruction technique used and may be influenced by the detectability of pathology. The H30 kernel with higher values of CNR indicates that it is better to use the H30 kernel when imaging the brain, because of the low contrast in the brain tissues.

At constant kVp, it was observed that CNR increased as the tube current (mAs) increased except at 210 mAs. This is not in agreement with Choi [18], who estimated that the value of CNR increased as tube current increased in all diameters of the phantom.

From **Figure 12(a)**, both the 10% and 50% spatial frequency appear to be linear with no significant difference in MTF. Additionally, **Figure 12(b)** showed an increase in image quality for both spatial frequencies from 13.7 mGy to 29.7 mGy and slowly decreased at 32.8 mGy. There was a sharp decrease at 36mGy and an increased at 39.1 mGy. There was no change in MTF value after 1.08 and radiation dose at 29.7 mGy.

This gives a clear indication that the H60 kernel (sharp kernel) gave a higher MTF value than the H30 kernel (smooth kernel). The sharp kernel thus has better spatial resolution than the smooth filter. This is good for imaging bony structures. Since the head is made of soft tissues and bony tissues. To visualise fracture in the bone, the H60 will be more appropriate. The reconstruction kernel used affects the ability of the imaging system to differentiate objects in the two spatial dimensions of an image. At 10%, there were higher MTF values than at 50%; this also indicates that spatial frequency affects MTF.

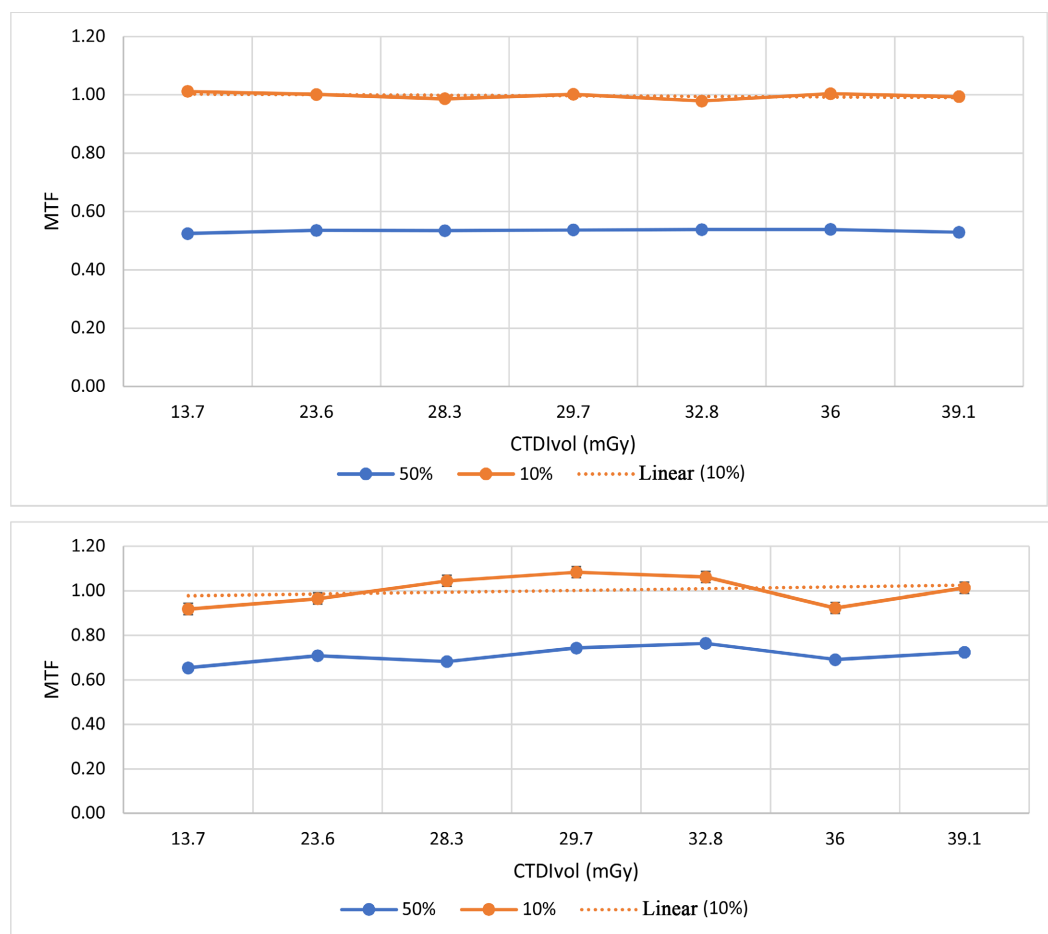


Figure 12. A graph of MTF and CTDI_{vol} with a pitch of 0.9 using (a) H30 kernel and (b) H60 kernel.

Skewing of the H60 kernel to the right and H30 kernel to the left implies that the H60 kernel had sharper images even though they were noisier. Thus, the closer the NPS peak is to the right, the sharper the image appearance; in other words, the images will have a fine grainy appearance. The H30 kernel had a lower NPS value and the images appeared smoother but were not sharp. This is good for imaging bony structures. Since the head is made of soft tissues and bony tissues. To visualise fracture in bone, the H60 will be more appropriate.

The eye lens received the highest dose while the thyroid received the lowest dose for both pitches. This is consistent with the findings of Roslee [20], who reported that the eye lens consistently received the highest cumulative dose when compared with the other organs. It was observed that the 0.9 pitch measured a lower dose of 35 mGy to the eye lens than the 0.5 pitch which measured 63 mGy of dose. It was realised that the higher the pitch the smaller the dose and this might be because of the faster table and gantry movement. Dose efficiency increases with smaller slice thickness and the pitch value is also high for small slice thickness. The 0.9 pitch measured a lower dose of 1.3 mGy to the thyroid while the 0.5 pitch measured a dose of 2.3 mGy.

5. Conclusion

The 0.9 pitch gave a lower radiation dose than the 0.5 pitch with a percentage reduction of 2.3%. The H30 kernel (smooth kernel) gave higher values for noise and CNR than the H60 (sharp kernel) which values were also high for modulation transfer function and noise power spectrum. CNR increases steadily as the $CTDI_{vol}$ increases and noise decreases as the $CTDI_{vol}$ increases. The eye lens received the highest radiation dose, while the thyroid received the least radiation dose.

Acknowledgements

The authors wish to thank St. Olavs Hospital (Trondheim, Norway) and the NORPART Project for their support during the study.

Conflicts of Interest

The authors declare no conflicts of interest regarding the publication of this paper.

References

- [1] Stephen, P.P., Fiachra, M., Maria, T., Karl, J., Owen, J.O.C. and Maher, M.M. (2016) Computed Tomography and Patient Risk: Facts, Perception and Uncertainties. *World Journal of Radiology*, **8**, 902-915. <https://doi.org/10.4329/wjr.v8.i12.902>
- [2] Triantopoulou, S. and Tsapaki, V. (2017) Does Clinical Indication Play a Role in CT Radiation Dose in Pediatric Patients? *Physica Medica*, **41**, 53-57. <https://doi.org/10.1016/j.ejmp.2017.03.014>
- [3] Sodhi, K.S., Krishna, S., Saxena, A.K., Sinha, A., Khandelwal, N. and Lee, E.Y. (2015) Clinical Application of "Justification" and "Optimization" Principle of ALARA

- in Pediatric CT Imaging: “How Many Children Can Be Protected from Unnecessary Radiation?” *European Journal of Radiology*, **84**, 1752-1757.
<https://doi.org/10.1016/j.ejrad.2015.05.030>
- [4] Hagelstein, C., Henzler, T., Haubenreisser, H., Meyer, M., Sudarski, S., Schoenberg, S.O., et al. (2016) Ultra-High Pitch Chest Computed Tomography at 70 kVp Tube Voltage in an Anthropomorphic Pediatric Phantom and Non-Sedated Pediatric Patients: Initial Experience with 3(rd) Generation Dual-Source CT. *Zeitschrift für Medizinische Physik*, **26**, 349-361. <https://doi.org/10.1016/j.zemedi.2015.11.002>
- [5] Trattner, S., Pearson, G.D.N., Chin, C., Cody, D.D., Gupta, R., Hess, C.P., et al. (2014) Standardization and Optimization of CT Protocols to Achieve Low Dose. *Journal of the American College of Radiology*, **11**, 271-278.
<https://doi.org/10.1016/j.jacr.2013.10.016>
- [6] Noferini, L., Taddeucci, A., Bartolini, M., Bruschi, A. and Menchi, I. (2016) CT Image Quality Assessment by a Channelized Hotelling Observer (CHO): Application to Protocol Optimization. *Physica Medica*, **32**, 1717-1723.
<https://doi.org/10.1016/j.ejmp.2016.11.002>
- [7] Weinman, J.P., Mirsky, D., Jensen, A.M. and Stence, N.V. (2019) Dual Energy Head CT to Maintain Image Quality While Reducing Dose in Pediatric Patients. *Clinical Imaging*, **55**, 83-88. <https://doi.org/10.1016/j.clinimag.2019.02.005>
- [8] Zarb, F., Rainford, L. and McEntee, M.F. (2010) Image Quality Assessment Tools for Optimization of CT Images. *Radiography*, **16**, 147-153.
<https://doi.org/10.1016/j.radi.2009.10.002>
- [9] Li, K., Garrett, J., Ge, Y. and Gh, C. (2014) Statistical Model Based Iterative Reconstruction (MBIR) in Clinical CT Systems. Part II. Experimental Assessment of Spatial Resolution Performance. *Medical Physics*, **41**, Article ID: 071911.
<https://doi.org/10.1118/1.4884038>
- [10] Rogers, L. (2001) Radiation Exposure in CT: Why So High? *AJR American Journal of Roentgenology*, **177**, 277. <https://doi.org/10.2214/ajr.177.2.1770277>
- [11] Berrington de Gonzale, A., Mahesh, M., et al. (2009) Projected Cancer Risks from Computed Tomographic Scans Performed in the United States in 2007. *Archives of Internal Medicine*, **169**, 2071-2077. <https://doi.org/10.1001/archinternmed.2009.440>
- [12] Brisse, H.J. (2009) The Relevance of Image Quality Indices for Dose Optimisation in Abdominal Multi-Detector Row CT in Children: Experimental Assessment with Pediatric Phantoms. *Physics in Medicine & Biology*, **54**, 1871.
<https://doi.org/10.1088/0031-9155/54/7/002>
- [13] Naumann, D.N., Raven, D., Pallan, A. and Bowley, D.M. (2014) Radiation Exposure during Paediatric Emergency CT: Time We Took Notice? *Journal of Pediatric Surgery*, **49**, 305-307. <https://doi.org/10.1016/j.jpedsurg.2013.11.044>
- [14] Ramos, S.M.O., Thomas, S., Berdeguez, M.B.T., Vasconcellos de Sá, L. and Sousa, S.A. (2017) Anthropomorphic Phantoms-Potential for More Studies and Training in Radiology. *International Journal of Radiology & Radiation Therapy*, **2**, 101-104.
<https://doi.org/10.15406/ijrrt.2017.02.00033>
- [15] Gundogdu, S., Mahmutyazicioglu, K., Ozdemir, H., Savranlar, A. and Asil, K. (2005) Assessment of Image Quality of a Standard and Three Dose-Reducing Protocols in Adult Cranial CT. *European Radiology*, **15**, 1959-1968.
<https://doi.org/10.1007/s00330-004-2550-7>
- [16] Hanan, E., Hussein, A.H., Ahmed, M., Hamid, O., Sultan, A. and Ali, Y. (2017) Assessment of Image Quality Parameters for Computed Tomography in Sudan. *Open Journal of Radiology*, **7**, 75-84. <https://doi.org/10.4236/ojrad.2017.71009>

-
- [17] Zhang, D., Gao, Y., Eckerman, X. and Liu, B. (2013) A method to Acquire CT Organ Dose Map Using OSL Dosimeters and ATOM Anthropomorphic Phantoms. *Medical Physics*, **40**, Article ID: 081918. <https://doi.org/10.1118/1.4816299>
- [18] Choi, H.R., Kim, R.E., Heo, C.W., Kim, C.W., Yoo, M.S. and Lee, Y. (2018) Optimization of Dose and Image Quality Using Self-Produced Phantom with Various Diameters in Pediatric Abdominal CT Scan. *Optik*, **168**, 54-60. <https://doi.org/10.1016/j.ijleo.2018.04.066>
- [19] Yu, L. (2016) Image Reconstruction Techniques. Image Wisely.
- [20] Roslee, M.A.A.M., Shuaib, I.L., Napi, A.F.M., Razali, M.A.S.M. and Osman, N.D. (2020) Cumulative Organ Dose and Effective Dose in Adult Population Underwent Repeated or Multiple Head CT Examination. *Radiation Physics and Chemistry*, **166**, Article ID: 108465. <https://doi.org/10.1016/j.radphyschem.2019.108465>.